Shear induced Reynolds stress at the edge of L-mode tokamak plasmas

N. Fedorczak[1], P.H. Diamond[1,2,3], G. Tynan[1], P. Manz[1]

[1] Center for Momentum Transport and Flow Organization, University of California at San Diego, San Diego, California 92093, USA

[2] WCI Fusion Theory, National Fusion Research Institute, 52, Yeoeun-dong, Yusung-Gu, Daejon, Republic of Korea

[3] CASS and Dept. of Physics, University of California San Diego, La Jolla, CA 92093-0429, USA

E-mail: nfedorczak@ucsd.edu

Abstract. The turbulent flux of momentum - or Reynolds stress - is a mechanism responsible for the generation of sheared flow by turbulence. The structure of the flux surface averaged stress $\langle \tilde{v}_r \tilde{v}_\perp \rangle$ is investigated in the edge region of a L-mode tokamak plasma. The stress induced by the perpendicular tilting of ballooning modes is considered. Besides the tilting by the $E \times B$ flow shear, which is a negative viscosity effect, a magnetic shear induced Reynolds stress - called $\hat{s}$-residual stress- arises as a consequence of a residual spatial tilting of ballooning modes by the magnetic shear in a poloidally up-down asymmetric magnetic geometry. A model is derived in the weak flow shear regime under the approximation of circular flux surfaces. The amplitude of this residual stress is of the order of the square of the radial velocity fluctuations in the scrape-off layer, and in the immediate radial vicinity of the separatrix if an X-point exists. Its amplitude drops rapidly to zero toward the plasma core, thus appearing as a source of transverse rotation at the interface. Its non-linear dependence on the electric shear is discussed in the context of weak electric shear

effect on the poloidal shape of the ballooning envelope. The local $\hat{s}$-residual stress is non uniform poloidally and changes sign according to the up/down position of scrape-off layer end-plates with respect to the $\nabla B \times B$ direction. The electric and magnetic shear induced stresses are then included in a flux surface averaged 1D model of mean flow conservation at the plasma edge, including the scrape-off layer volume. In L-mode weak shear regimes, it is shown that changing the plasma geometry from $\nabla B \times B$ away from the divertor to $\nabla B \times B$ toward the divertor approximately double the electric shear strength inside the separatrix, as reported in experiments. This shear induced stress also enters the toroidal momentum balance, where it appears as a significant source of momentum in the immediate vicinity of the separatrix. Balanced by the toroidal viscosity only, it can sustain toroidal flow gradients in the order of a km.s^{-1}.cm^{-1} at the separatrix, with a sign also dependent on the plasma geometry. These momentum sources arising from symmetry breaking at the boundary of the confined region may explain why low to high mode power thresholds are lower in favorable than unfavorable configurations, and may be important for the issue of optimal plasma shapes with respect to edge intrinsic shear.

PACS numbers: 52.55.Fa, 52.25.Xz,52.30.-q, 52.35.Ra, 52.40.Hf, 52.55.-s

Sheared flows at the edge of Tokamak plasmas have been a research subject of critical importance for decades. As a matter of fact, the energy and particle confinement in a tokamak can increase dramatically at the transition from so called low (L) to high (H) confinement regimes characterized by the onset of a strong transverse velocity shear in the vicinity of the separatrix (see [1] and a review in [2]). Crudely, if the shearing rate surpasses the growth rate of plasma instabilities, turbulent eddy decorrelation is said to reduce the transport of particles and energy across the sheared region [3], thus allowing local gradients to build up [4] [5]. This scenario is important for achieving a burning plasma in ITER, and for this reason has been the focus of numerous experimental and theoretical works. Recent understanding [3] of the L-H transition has suggested a multi-step process for the onset of the transport barrier [6] [7] [8] [9] in given plasma regimes : in L-mode, the local turbulence and zonal flow (sheared flow generated by turbulence) become elements of an oscillating predator-prey regime (or limit cycle). To complete the dynamics, the ion pressure gradient responds to the quenching of turbulent transport [10] and so enters the predator-prey system through the equilibrium radial electric field that is associated with the pressure gradient, which is also the source of free energy for the turbulence activity. Eventually the system reaches a stage where the zonal flow grows and the turbulence activity is reduced, which allows the energy in the mean flow associated with the pressure gradient to increase. This then suppresses the turbulence (and zonal flow shearing), allowing the edge pressure gradient to steepen rapidly. This signifies that the L to H mode transition occurred.

Though simple models are now able to capture this limit cycle transition to an H-mode like edge plasma, they indeed remain simplified models in the sense that their prediction capabilities are

limited by the incomplete description of zonal flow drive mechanisms. As described in [1], the drive of zonal flow by the Reynolds stress originates from a radial group velocity of potential or magnetic field fluctuations. The structure of the Reynolds stress, and the physical mechanisms behind the dispersion relation and group velocity, will enter the limit-cycle dynamics, and also define the initial state of the flow through the initial equilibrium radial electric field it supplies in the L-mode. Experiments show that H mode transport barriers develop above a mean shear flow strength [6], and stronger initial sheared flow regimes exhibit lower L-H transition power threshold [11]. This is thought to be a reason why the L-H transition requires a large amount of additional power when $B \times \nabla B$ is away from the X-point (unfavorable geometry) as compared to when it points toward the X-point (favorable geometry) [12] [11]. Indeed L-mode velocity measurements show that the edge $E \times B$ shear is stronger in the favorable geometry than for the unfavorable [13], when other discharge parameters are matched. For circular plasmas limited by a poloidally localised and toroidally uniform limiter, the analogy is possible by replacing X-point position by limiter position. Although these limited plasmas do not present common L to H mode transitions, the L-mode transversal rotation profile in the vicinity of the last closed flux surface (LCFS) is also observed to depend on the position of the limiter with respect to $B \times \nabla B$ direction [14]. The up-down position of the X-point is not the only geometrical factor which impacts the L-H transition. The threshold is also observed to depend on the radial position of the X-point (lower triangularity) in NSTX [15]. The issue of why the magnetic topology has an influence on the L-mode edge radial electric field should be seriously considered for its critical impact on the definition of plasma geometries optimizing the L-H power threshold.

Stringer *et al.* proposed an instability mechanism [16][17] for the spin-up of core parallel rotation, arising from the ballooning of the radial particle flux on magnetic flux surfaces supporting asymmetric density perturbations. Labombard *et al.* [18] then extended the model in the scrape-off layer (SOL) where the ballooning of the particle flux across the last closed flux surface is experimentally evident [19, 20, 21, 22, 23]. Labombard, then Gunn, demonstrated the existence of Stringer-like parallel flows in the SOL volume, driven from the outboard midplane to the divertor end-plates where particle sinks are located. L-mode discharges in C-mod with the $\mathbf{B} \times \nabla B$ directed toward (away from) the X-point exhibit a co-current (counter current) volume-averaged toroidal momentum in the SOL. Comparable observations are made on limiter circular plasmas in Tore Supra [19]. These quasi-sonic flows may propagate inward and drive the confined parallel rotation. In the core region, a radial flux of parallel momentum has been investigated in gyrokinetic simulations by Camenen *et al.* [24]. A non-diffusive and non-convective flux arises from the up-down asymmetry of ballooning modes on asymmetric flux surfaces. They highlighted that a similar effect should exist for the transversal rotation.

Extending these previous works about the effect of poloidal asymmetry, we propose that ballooning transport at and just inside the LCFS gives rise to a local turbulent Reynolds stress $\langle v_r v_\perp \rangle$ that depends on the magnetic and $E \times B$ shear. Poloidal asymmetry of the magnetic shear dependence then yields a net Reynolds stress, which in turn impacts the $E \times B$ flow profile. The source of momentum associated with this stress is particularly strong at the separatrix but has never been considered before in that region for it's role in the onset of L-mode shear layer and source of toroidal rotation at the boundary of the confinement region.

The body of this paper is organized as follows. In the first section we introduce the local Reynolds stress induced by the tilting of electrostatic ballooning modes. In the second section we describe a simplified model for the influence of magnetic geometry and electric shear flow on the ballooning envelope across the separatrix. The magnetic geometry constrains the envelope amplitude to zero in the vicinity of the X-point, and in the low shear flow limit the envelope is poloidally shifted by the electric shear. In a third section, an expression of the flux surface averaged magnetic shear induced Reynolds stress is proposed in the limit of circular flux surfaces and weak electric shear. The dependence on the electric shear flow shows a non zeros offset, which is on the order of the square of the fluctuating radial velocity amplitude. Its sign reverses with the reversal of the up-down asymmetry ($\mathbf{B} \times \nabla B$ toward or away from the X-point). In the fourth section, the shear induced stress is inserted in a simplified momentum conservation model in the low shear limit. We show that for relevant L-mode tokamak plasma parameters the mean flow shear in favorable geometry can be up to 2 times higher than in unfavorable one. We conclude with a discussion on the existence of a residual stress for the toroidal rotation, which is a geometrical consequence of the shear induced stress for the perpendicular rotation.

1. Reynolds stress associated with electrostatic ballooning modes

Ballooning modes refer to instabilities associated with the curvature of the magnetic field which results on the local polarization of pressure eddies from diamagnetic currents. In the outer outer-half of the plasma cross section, the polarization is destabilizing whereas it is stabilizing in the inner-half. For instance, the destabilizing contribution of the diamagnetic polarization to the local

growth rate of an ideal interchange mode k_r, k_θ is proportional to the local curvature [25]:

$$\gamma^2 \propto \frac{(\nabla B \times \mathbf{B})_\theta}{B^2} \frac{k_\theta^2}{k_\theta^2 + k_r^2} \tag{1}$$

where diffusion damping, parallel currents and polarization currents have been intentionally omitted. The curvature term is a projection along the poloidal direction, which depends on the poloidal position $(\nabla B \times \mathbf{B})_\theta \propto \cos\theta$ in the circular geometry approximation. Note that we also considered a weak poloidal rotation frequency of the plasma, which would act as an effective temporal modulation of the geometrical curvature during the growth phase. Without poloidal variation of the wave number, the local growth rate is peaked at the outboard midplane $\theta_0 = 0$ and vanishes rapidly away from this position. In the linear phase of the mode evolution, density and polarization grow initially in a narrow poloidal section of the plasma, centered on the poloidal position θ_0. At the same time the parallel dynamics spread the mode structure along the flux tube, into regions where the diamagnetic current acts to damp the polarization. Two properties arise from these simplified dynamics: (1) the mode exhibits a parallel or ballooning envelope centered at the most unstable location θ_0, of width partially fixed by the poloidal variation of the curvature excitation, (2) the mode exhibits a flux tube geometry defined at the most unstable location and *constrained elsewhere by helicity and magnetic flux expansion.* This differential helicity is parametrized by the magnetic shear which is defined as the inverse of helicity gradient scale length normalized by the minor radius of the flux surface $\hat{s} = \frac{r}{q}\partial_r q$ where q is the safety factor. Away from the outboard midplane, the magnetic shear progressively tilts the mode in the transversal plan (see figure 2). This effect has been reported in 3D simulations of electrostatic ballooning modes [26] and also in SOL experiments [27, 28]. The local electric shear $V'_E \equiv \partial_r V_E$ will also tilt the modes by a progressive differential convection of density and vorticity [29]. Representation of these tilting effect in terms of mode wave vector is addressed below, considering the following geometrical conventions. The local radial direction (supported by the unit vector e_r) is directed from the plasma core to the edge, normal to the flux surfaces. The transverse (poloidal) direction $\perp$ (θ) is oriented along $B \times e_r$. A positive radial electric field gives always rise to a negative transversal drift. Finally,

we consider the limit of weak magnetic flux expansion, so that the transversal wave number stays constant along a flux tube : $k_\perp(\theta) = k_\perp(0)$.

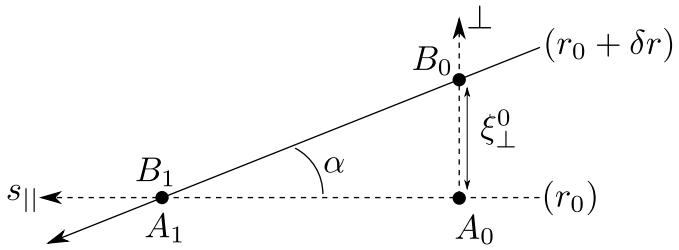

Figure 1. Schematic of two field lines lying at two radial positions r_0 and $r_0 + \delta r$. The transverse direction $\perp$ is considered at the position r_0. The points A_1 and B_1 lie respectively at r_0 and $r_0 + \delta r$, at the same transverse and toroidal position. A_0 and B_0 lie respectively at r_0 and $r_0 + \delta r$ at the same parallel position but transversally separated by $\xi_\perp^0$ (according to r_0 axes)

In an Eikonal representation of the mode structure, the wave vector is generally defined by the gradient of the complex phase of the mode : $k = \nabla\varphi$. Let us consider a reference flux surface at the radius r_0, where the transversal electric flow is by definition zeros. On a second flux surface radially separated by δr, the transversal flow is written as $V_E = V_E'\delta r$ where V_E' is the flow shear. Considering A_1 and B_1 at a given parallel position s_1 and aligned along the radial vector - as pictured on figure 1, the local radial wave number is approximated by : $k_r(s_1, t) = \frac{\varphi(B_1,t)-\varphi(A_1,t)}{\delta r}$. Because of the flux tube geometry of the mode, the phase is uniform along magnetic field lines. Thus considering two other points A_0 and B_0 on the respective field lines but at the parallel position s_0, the radial wave number at the position s_1 is also given by : $k_r(s_1, t) = \frac{\varphi(B_0,t)-\varphi(A_0,t)}{\delta r}$. Written in the $(r, \perp, s, t)$ coordinate system: $\varphi(A_0, t) = \varphi(r_0, 0, s_0, t) = \varphi(r_0, 0, s_0, 0)$ since there is no convection on the reference flux surface, and $\varphi(B_0, t) = \varphi(r_0 + \delta r, \xi_\perp^0, s_0, t) = \varphi(r_0 + \delta r, \xi_\perp^0 - V_E' t\delta r, s_0, 0)$ by correcting the

transverse position by the convection of the mode on the second flux surface. The transversal displacement between A_0 and B_0 is related to the difference of helicity between the two field lines : $\xi_\perp^0 = \frac{s_1-s_0}{q(r_0)^2}\left[q(r_0+\delta r)-q(r_0)\right] = \delta r(s_1-s_0)\frac{\hat{s}}{r_0 q(r_0)}$. Now considering the parallel position s_0 as a reference of the flux tube where the phase is defined by the initial wave vector of the ballooning mode $k_{t=0} = (k_r^0, k_\perp)$, we obtain $\varphi(B_0,t)-\varphi(A_0,t) = k_r^0\delta r + k_\perp\left[\xi_\perp^0 - V_E' t\delta r\right]$, so that the local radial wave vector at the time t and parallel position s_1 is given by $k_r(s_1,t) = k_r^0 + k_\perp\left[\hat{s}\frac{(s_1-s_0)}{r_0 q(r_0)} - V_E' t\right]$. The poloidal displacement is defined by $\theta-\theta_0 = \frac{(s_1-s_0)}{r_0 q(r_0)}$, which gives the following tilting relation for the wave vector after a mode life time τ_c:

$$\begin{cases} k_\perp(\theta) &= k_\perp(\theta_0) \\ k_r(\theta) &= k_r(\theta_0) + \left[(\theta-\theta_0)\hat{s} - V_E'\tau_c\right]k_\perp \end{cases} \tag{2}$$

Considering θ_0 as the ballooning peaking position without electric shear and noticing that the growth rate is maximum for minimum k_r, we will consider in the following $k_r(\theta_0) = 0$. It will be also assumed that $\theta_0 = 0$, i.e. that the instability is centered at the outboard midplane without electric shear. A linear relation between the electrostatic drifts $\tilde{v}_r$ and $\tilde{v}_\perp$ follows naturally from the local dispersion relation given by Eq.2: $\partial_r\tilde{\phi} = \left[\theta\hat{s} - V_E'\tau_c\right]\partial_\perp\tilde{\phi}$, or equivalently $\tilde{v}_\perp = -\left[\theta\hat{s} - V_E'\tau_c\right]\tilde{v}_r$. As shown in [28], if one could experimentally measure the turbulent poloidal flux $\langle\tilde{v}_\perp\tilde{n}\rangle$ away from the midplane ($\theta \neq \theta_0$) at the edge of tokamak plasmas, one would surely find a time averaged value directed toward the outboard midplane and approximately proportional to the radial flux amplitude and the poloidal angle as a consequence of the magnetic shear tilting in the case of weak electric shear. Equivalently, this local orientation of the mode velocity is identifiable as a factor in the Reynolds stress $\tilde{v}_r\tilde{v}_\theta$. Its amplitude should also be modulated by the ballooning envelope of the potential perturbation $\tilde{\phi}(\theta) = \tilde{\phi}(0)F_\phi(\theta)$. The local time averaged expression of the radial

flux of transversal momentum is:

$$\langle \tilde{v}_r \tilde{v}_\perp \rangle_t = \left\langle \tilde{v}_r^2(0) \right\rangle_t F_\phi^2(\theta) \left[-\theta \hat{s} + V_E' \tau_c \right] \tag{3}$$

The second RHS term refers to the electric shear induced Reynolds stress, a negative viscosity flux $\Pi_{V_E'} = -\chi_{eff} \partial_r V_E$ with $\chi_{eff} = -\langle \tilde{v}_r^2 \rangle_{t,\theta} \tau_c$. Note however that it acts only on the electrostatic component of the flow $V_E = V_\perp - V^*$, which means that within the common definition of viscosity acting on the total flow, the diamagnetic contribution should appear as a residual stress, i.e $\langle \tilde{v}_r \tilde{v}_\perp \rangle_{dia} = -\langle \tilde{v}_r^2 \rangle_{t,\theta} \tau_c \partial_r V^*$. Nevertheless, the initial expression of the electric shear induced Reynolds stress given by Eq.3 is retained in the following. The first term on the RHS is the magnetic shear induced Reynolds stress $\Pi_{\hat{s}}$, which is apparently neither proportional to the mean flow nor its gradient, and so is referred as to an apparent *residual stress*. This stress depends strongly on the poloidal position along a flux surface via the term $\theta F_\Phi^2(\theta)$, in comparison to the electric shear induced stress that depends only in the local envelope amplitude $F_\Phi^2(\theta)$. It is an odd function of θ unless the ballooning envelope is not poloidally symmetric, which is the necessary condition to obtain a non vanishing poloidal average of $\Pi_{\hat{s}}$. We address this case in the following, considering in addition the effect of weak electric shear on the position of the envelope. Following discussions about the effect of an X-point on the geometry of magnetic flux tubes are based on an analytic description of the magnetic field as given in [30].

2. Asymmetric ballooning envelope with a sheared flow

A quantitative investigation of the magnetic shear induced Reynolds Stress requires the ballooning envelope response to geometrical shaping of the flux surfaces and to a electric shear flow. The first

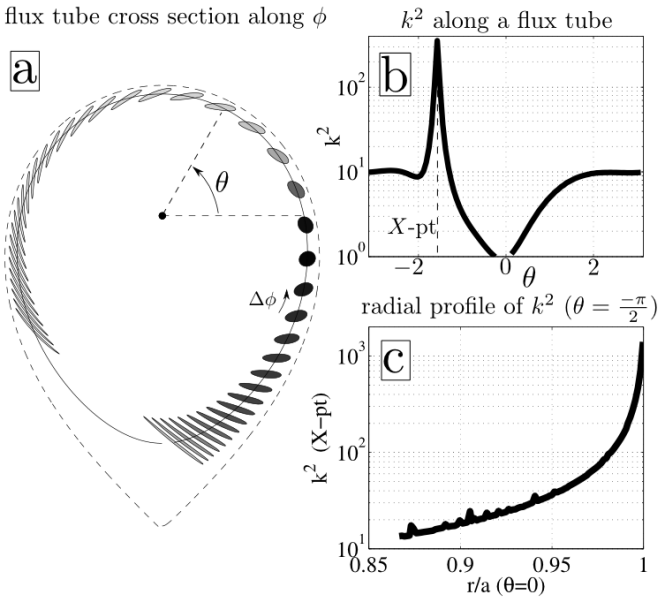

Figure 2. **a**: poloidal cross section of a lower-single-null shaped plasma. A circular flux tube is started around the outboard midplane and its cross section is mapped along the field line at a fixed toroidal increment. The magnetic shear effect is noticeable over the whole surface, and the flux expansion close to the X-point. **b**: poloidal evolution of a flux tube transversal wave vector ($k^2 = 1$ at outboard midplane) on an edge flux surface. Note the exponential growth at the vicinity of the X-point location. **c** : Radial profile of the wave vector expansion at the x-point location for a wave vector $k^2 = 1$ at the outboard midplane

point is addressed in [31] and the second is discussed in [32]. Two basic features are retained in the following for the analytic derivation of the first order components of the magnetic shear induced Reynolds stress. Toward the core, the ballooning envelopes are almost poloidally symmetric as a consequence of the symmetry of the magnetic flux surfaces. In the scrape-off layer, the end-plates bound the parallel extent of the modes, creating a net poloidal asymmetry of the ballooning envelope. In the case of circular and toroidally limited plasmas, this creates a radial gradient of $\Pi_{\hat{s}}$ at the LCFS which can therefore drive the transversal rotation their. The magnetic field ripple

will be responsible for the finite width of the transition area, that defines also the typical scale length of the stress gradient. In the case of diverted geometries, an additional effect appears at the boundary volume of the confined region due to the presence of an X-point. As illustrated on figure 2 and documented in [31], the magnetic flux expansion in the direct vicinity of the X-point volume is responsible for the exponential increase along the field line of the wave vector of a ballooning mode excited at the outboard midplane. In other words the turbulent decorrelation of the mode $\propto Dk^2$ can totally damp the mode amplitude in the direct vicinity of the X-point, which is totally equivalent to the scrape-off layer symmetry breaking. Note that the exponential enhancement of wave vector vanishes extremely rapidly as the radial position is moved toward the core. Regarding the sharp poloidal asymmetry of a ballooning envelope, a sharp transition takes place between the confined region and the scrape-off layer for both toroidally limited and diverted plasma geometries. The asymmetry of the envelope is in fact associated with the existence of a net tilt of the mode due to the magnetic shear. As illustrated on figure 2a the tilt induced at the position opposite to the X-point location dominates on the flux surface. It is important to mention now that changing the up/down position of the X-point relative to the magnetic field direction will reverse the sign of this residual tilt, therefore reversing the sign of the magnetic shear induced Reynolds Stress. In the following these effects will be treated given a synthetic description of the ballooning envelopes truncated at the X-point position. Generally the magnetic field curvature $(\nabla B \times \mathbf{B})_\theta$ is poloidally asymmetric on shaped magnetic flux surfaces, resulting in asymmetries of the ballooning envelope [24]. Adding these asymmetric envelope components besides the main X-point truncation are in principle important of the detail of the stress, but omitting them will not modify the basic results

related to the X-point position. In the following, a circular flux surface approximation is followed. Ballooning envelopes will be represented by a Gaussian function truncated at the X-point position, which is a reasonable description at the edge of circular plasmas [20, 21].

The effect of weak electric shear on the envelope is now addressed. Inserting the radial wave vector expression (Eq.2) in the local growth rate of the ballooning mode (Eq.1) gives:

$$\gamma^2 \propto \frac{(\nabla B \times \mathbf{B})_\theta}{B^2} \frac{1}{1 + [\hat{s}\theta - V'_E \tau_c]^2}$$

In the absence of electric shear, the maximum growth rate is at the outboard midplane $\theta = 0$. For a finite value of V'_E, the position of minimal k_r and maximal growth rate is shifted poloidally as a result of the local balance between magnetic and electric shear:

$$\theta_0(V'_E) \approx \frac{V'_E \tau_c}{\hat{s}} \tag{4}$$

This effect is observed in global simulations as mentioned in [33]. In fact the mode starts growing at the outboard midplane, where the curvature effect is maximal. During the growth phase, the electric shear will progressively modify the local wave number, thus impacting the local growth rate. After τ_c, the position of maximum growth has been progressively shifted from $\theta = 0$ to $\frac{V'_E \tau_c}{\hat{s}}$. Treated rigorously, the progressive displacement of the minimum wave vector position will induce a progressive poloidal asymmetry of the envelope, in analogy to the asymmetry of the curvature. Again this effect is not retained, and we only consider a bulk displacement of the Gaussian envelope to the peaking position $\theta_0 = \frac{V'_E \tau_c}{\hat{s}}$, as illustrated on figure 3. The weak shear regime can be understood as a condition on the maximum poloidal displacement of the envelope, typically $\left|\frac{V'_E \tau_c}{\hat{s}}\right| < 0.5$.

3. Synthetic derivation of $\Pi_{\hat{s}}$ expression

Given the shape of the ballooning envelope, we can estimate the different terms in the shear induced Reynolds stress as given by Eq.3. For convenience, the poloidal position is defined in the domain $\theta \in [-2\pi, 2\pi]$, since the inboard side of the X-point location must be accessible from the outboard midplane. The X-point location will be $\theta_X = +\pi/2$ in unfavorable geometry and $\theta_X = -\pi/2$ in favorable geometry, the latter case considered in the following. The Gaussian envelope centered on θ_0 is noted $F_{\theta_0}(\theta) = \exp\left[-\left(\frac{\theta-\theta_0}{\Delta\theta}\right)^2/2\right]$ where the width $\Delta\theta$ is a tunable parameter. The poloidal truncation of the mode envelope means that the inner part of the poloidal domain is determined by connection to the plasma crown (see figure 3 **a**), so that the mode is continuous on the domain $[\theta_0 \to 2\pi + \theta_X]$ (crown) and $[\theta_0 \to \theta_X]$ (directly toward the X-point). An apparent discontinuity at $\theta = \theta_X \pm \delta$ is solved in the confined region by realizing that the mode amplitude exponentially vanishes while approaching the X-point from both poloidal directions. In the SOL, there is no discontinuity since the field lines are not closed. In practice, the poloidal averages present in the Reynolds stress expression contain the asymmetry through the spatial boundaries of the integral :

$$\langle A \rangle_\theta \equiv \frac{1}{2\pi} \int_{\theta_X}^{2\pi+\theta_X} A d\theta$$

Before going further a discussion on the practical treatment of the radial and poloidal asymmetries in the Reynolds stress is required. As expressed by Eq.3, the local Reynolds stress can be rewritten as proportional to $\langle \tilde{v}_r \tilde{v}_\perp \rangle_t \propto F_{\theta_0}(\theta)\,[\theta_0 - \theta]\,\hat{s}$ where the electric shear component has been hidden in the peaking position θ_0. Indeed considering that the envelope is shifted poloidally is equivalent to consider that the tilt of the mode is only due to the magnetic shear acting along field lines from the shifted peaking position. Keeping explicit the negative viscosity contribution in the

poloidal average of the Reynolds stress then leads to $\langle \tilde{v}_r \tilde{v}_\perp \rangle_{t,\theta} \propto \langle F_{\theta_0}^2 \rangle V'_E \tau_c - \langle \theta F_{\theta_0}^2 \rangle_{t,\theta} \hat{s}$. The negative viscosity is supposed to take place on every flux surface without influence of the poloidal symmetry breaking. On the other hand the magnetic shear contribution is only effective at the very edge where the envelope is asymmetric, and is considered to vanish rapidly toward the core. In practice, for a given plasma configuration, this effect is implemented in the stress expression by adding a gate function $g_X(\rho)$ that varies radially from 0 in the core to 1 in the SOL. We end up with a calculable expression of the shear induced Reynolds stress along the radial position:

$$\langle \tilde{v}_r \tilde{v}_\perp \rangle_{t,\theta} = g_X \underbrace{\langle \tilde{v}_r^2 \rangle_{t,\theta} \frac{-\langle F_{\theta_0}^2 \hat{s}\theta \rangle_\theta}{\langle F_{\theta_0}^2 \rangle_\theta}}_{\Pi_{\hat{s}}} + \underbrace{\langle \tilde{v}_r^2 \rangle_{t,\theta} V'_E \tau_c}_{\Pi_{V'_E}} \tag{5}$$

Through the dependence of the envelope function with the mean sheared flow, $\Pi_{\hat{s}}$ also depends on V'_E as illustrated on figure 3 **b**. In favorable geometry and for $V'_E = 0$, $\Pi_{V'_E}$ is zeros and $\Pi_{\hat{s}}$ is strictly negative. Indeed the negative contribution of the mode tilting at the plasma crown is larger than its contribution between the outboard midplane and the X-point. A positive electric shear will then shift the ballooning envelope toward the plasma crown, increasing the positive contribution of the mode tilting in the region between the X-point and the envelope center. In fact, the magnetic shear contribution to the Reynolds stress, $\Pi_{\hat{s}}$, decays with V'_E and shows an offset at zeros of the electric shear. This is the effective residual stress induced by the magnetic shear, or $\hat{s}$-residual stress. It is interesting to note that the rough linear decay of $\Pi_{\hat{s}}$ is equivalent to a positive viscosity effect, which moderates the influence of the negative viscosity. Within a more general approach $\Pi_{\hat{s}}$ can be considered as a fully non-linear function of the electric shear, making it a residual stress. As observed on figure 3 **b**, the slope of $\Pi_{\hat{s}}(V'_E)$ and the residual offset depend both on the poloidal width of the ballooning envelope, since the later characterizes the degree of

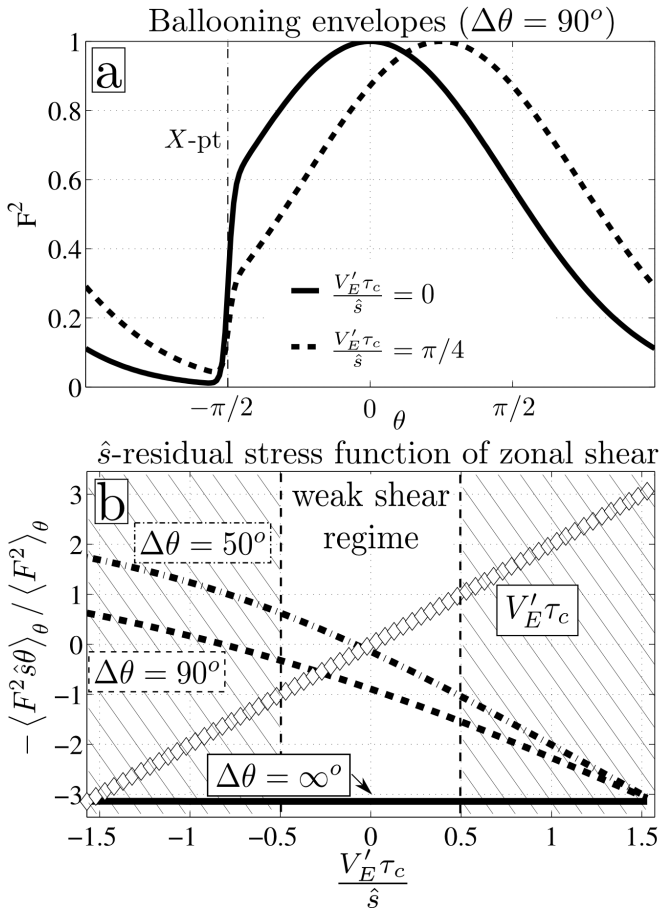

Figure 3. **a**: poloidal ballooning envelopes as Gaussian functions ($\Delta\theta = 90^o$), one shifted poloidally toward $\theta_0 = \pi/4$. The envelopes are truncated at the X-point located at $\theta_X = -\pi/2$. Note that the envelopes at $\theta < \theta_X$ are built by connection along the direction $\theta > 0$ opposite to the X-point location. **b**: $\Pi_{\hat{s}}$ stress function of the zonal shear for different synthetic envelopes truncated at $\theta_x = -\pi/2$ (favorable geometry). Is also shown the electric shear induced Reynolds stress (proportional to $V'_E\tau_c$). Note that the weak shear flow regime should only apply for small values of the electric shear in the range $|V'_E\tau_c/\hat{s}| < 0.5$.

asymmetry of the truncated envelope with respect to the peaking center. The effect of envelope width has also been investigated on gyrokinetic simulations by Camenen *et al.* in the context of parallel momentum flux [34]. In the extreme case of almost flute-like modes ($k_{||} \approx 0$ except at X-point location), $\Pi_{\hat{s}}$ does not depend on the electric shear and reaches its maximum strength. In

this case it is simply proportional to the X-point position angle $\Pi_{\hat{s}} \propto -\hat{s}\,(\pi + \theta_X)$. Extrapolating this linear dependence with the X-point position to all realistic ballooning width, we also find that the magnetic shear induced Reynolds stress should increases in amplitude with the triangularity.

In the case of unfavorable geometry, geometrical considerations are enough to derive a stress expression from the one derived in the favorable geometry. By inverting the flux surface geometry about the major radius axis, the magnetic shear stress changes sign. But since a positive electric shear would shift the envelope away from the X-point in favorable geometry, the latter is now shifted toward the X-point in unfavorable one, so that the dependence of $\Pi_{\hat{s}}$ with the sheared flow is also reversed:

$$\Pi_{\hat{s}}^{\text{unfav}}(V_E') = -\Pi_{\hat{s}}^{\text{fav}}(-V_E') \tag{6}$$

, which is also true for the negative viscosity component of the Reynolds stress. Note that there is no effect of the sign of the plasma current on the flux of transversal momentum.

It is important to mention that for realistic values of the envelope width, the flux of momentum $\Pi_{\hat{s}}$ is of the order of the square of the radial velocity fluctuations, and exhibits a strong radial variation through the weight function g_X. Since at the edge of a tokamak the electrostatic fluctuations dominate the particle and energy transport and so determine the L-mode pressure profile, this should have an important contribution to the source of L-mode poloidal rotation at the edge. In the following we illustrate the effect of $\Pi_{\hat{s}}$ and $\Pi_{V_E'}$ on the mean radial electric field profiles at the edge of L-mode plasmas with favorable and unfavorable geometries.

4. A model for perpendicular momentum conservation

The electric shear layer structure at the edge of an L-mode plasma can be understood as a result of the electric field penetration to the core from the SOL. Indeed *if no external torque is applied* as for intrinsic rotation studies, the neo-classical description of radial force balance in case of strong ripple predicts that core electric field is nearly proportional to the pressure gradient $E_r = \frac{T_i}{q}\left[\frac{\partial_r n_i}{n_i} + 3.37\frac{\partial_r T_i}{T_i}\right]$ [35], *and so directed inward*. The condition of strong ripple means that ion losses in local ripple mirrors is the dominant effect of radial flux ambipolarity, which is roughly true if the plasma has a finite collisionality and the core turbulent transport is weak. In sheath limited scrape off layer plasmas, the electric field is commonly observed to be proportional to the electron temperature gradient $E_r = -3\partial_r T_e$ [36], *and so directed outward*. This is due to an effect of sheath potential drop at the boundary of the field lines, although departure from the previouys relation are possible. The potential continuity from the core to the LCFS then naturally requires the formation of a sheared radial electric field in its vicinity. The role of the shear induced Reynolds stress in determining the position and shape of this shear layer is addressed below. That said, the effect of turbulence on the SOL radial electric field remains an open issue. For the seek of simplicity, we may consider that SOL electric field does only depends on temperature profile, which is likely to be questionnable especially at the immediate vicinity of the LCFS if the turbulence flow drive is strong at that location.

The dynamics of the edge radial electric field in the confinement region is described from a momentum conservation criterion. Neglecting electron mass, one writes the flux surface averaged

poloidal momentum conservation equation

$$\partial_t \langle n v_\perp \rangle_\theta + \partial_r \langle n v_r v_\perp \rangle_\theta = -n \nu_{cx} \langle v_\perp \rangle_\theta \tag{7}$$

where $v_\perp = \frac{E_r \times B}{B^2} - \frac{\nabla_r P_i \times B}{n q_i B^2}$ is the first order ion fluid drift. The RHS term describes the loss of momentum by charge exchange with neutrals. The LHS term $\partial_r \langle n v_r v_\perp \rangle_\theta$ corresponds to a local source of momentum. In general, this term could be decomposed into a diffusive part, a pinch part and a residual part, which here corresponds to our shear induced Reynolds stress. At the edge, the turbulent particle flux is rapidly varying and possibly acts as a mixing mechanism between neighbor flux surface. This exchange can be described by a diffusive process with a momentum transport coefficient comparable to the gyro-Bohm value:

$$\langle n v_r v_\perp \rangle_\theta = -\chi_\perp \partial_r \langle v_\perp \rangle_\theta + g_X \Pi_{\hat{s}} + \Pi_{V'_E}$$

Where $\chi_\perp \approx D_{GB}$. Adding a pinch contribution to the momentum flux will not change the basic results reported here. Now the time evolution of the poloidal momentum has a generic form, composed of: a linear damping, a diffusive flux, and a source of momentum defined here by the radial derivative of the shear induced Reynolds stress. The system is in general non linear, so that the stationary state should be given by an iterative solution starting from an initial profile. In fact, the non linearity is in general not only contained in the magnetic shear induced stress, but also appears through the dependence of the turbulence intensity on the electric shear, impacting transport coefficients and background density and temperature profiles. That said, our analyzes is limited to the weak shear regime, for which transport coefficients and plasma profiles are frozen. Therefore the momentum conservation equation reduces to the description of the time evolution

of the $E \times B$ velocity:

$$\partial_t V_E + \frac{1}{n}\partial_r \left[n \left(\Pi_{\hat{s}} + \Pi_{V_E'} \right) \right] = - \left[\nu_{cx} - \chi_\perp \partial_r^2 \right] \left(V_E + V_i^* \right) \tag{8}$$

Toward the core, gradients and momentum sources are generally weak, so that the solution of Eq.8 should satisfy $v_\perp = V_E + V_i^* = 0$, condition for ion radial force balance. As for the neo-classical prediction, we should recover that the radial electric field is nearly proportional to the pressure gradient $E_r = \frac{\nabla_r P_i}{nq}$. Approaching the last closed flux surface, the scrape-off layer is treated as a semi-rigid boundary condition. The ambipolarity of the radial flux in the confinement region do not apply in the SOL, since charges are free to re-circulate between the divertor and the plasma, i.e $\nabla \cdot J = 0$ involves parallel currents. The SOL electric field $E_r = -3\partial_r T_e$ is imposed as a boundary condition at the LCFS by applying an additional damping term to Eq.8 : $\partial_t V_E \rightarrow \partial_t V_E + \frac{\chi_{SOL}}{\tau_{SOL}} \left(V_E - V_E^{SOL} \right)$. V_E^{SOL} is the frozen SOL electric field and χ_{SOL} is a step function equal to 0 in the confined region and 1 in the SOL. The damping time τ_{SOL} is refers to a transport time through the SOL which is in principle much smaller than any time scale associated with source and sinks of momentum, such that the V_E profile is imposed frozen in the SOL. Relaxing this condition in the immediate vicinity of the LCFS is in principle required for the case of limiter plasmas, for which the Reynolds force is located at the LCFS. Applied to diverted configurations, this relaxation has minor impacts since the Reynodls force is mostly located in the confined region. Since SOL radial electric field remains an open issue beyond the scope of this paper, the approximation is done that results for limiter plasmas should not differ from results presented here for diverted plasmas, the main difference beeing in the radial position

of the Reynolds drive. The different parameters appearing in Eq.8 are chosen

$$\begin{aligned} \sqrt{\langle \tilde{v}_r^2(0) \rangle_t} &= 3.10^{-2} c_S \quad , \quad \chi_\perp = 0.5 \rho_S^2 \omega_S \\ \nu_{coll} &= 1.10^{-4} \omega_S \quad , \quad \tau_c^{-1} = 1.10^{-2} \omega_S \\ N_e^{LCFS} &= 4.10^{18} \mathrm{m}^{-3} \quad , \quad T_i^{LCFS} = 40 \mathrm{eV} \\ \tau_{SOL}^{-1} &= 1.10^{-1} \omega_S \end{aligned} \tag{9}$$

where c_S, ρ_S and ω_S are respectively the ion sound speed, the sonic Larmor radius and the sonic precession at the LCFS ($c_S = \rho_S \omega_S$). The velocity fluctuation amplitude is typically what is measured with probes in the near SOL and agrees with scalings proposed in [37], and the effective viscosity $\chi_\perp$ is in the Gyro-Bohm range. In particular we will also assume that the life time of the modes τ_c is constant, though it should be a function of the local flow shear [38] in case of strong shear. Note that the negative viscosity coefficient is also of order of gyro-Bohm. The frozen profiles of density and temperature are shown in figure 4. Typically, their radial decay lengths are a few centimeters at the separatrix, and increase to the order of the minor radius toward the core. The radial variation of $\Pi_{\hat{s}}$ due the radial variation of X-point resistivity, represented by g_X, is also shown in figure 4 **b**. It is one in the SOL, zero in the core and exhibits a sharp exponential increase 1 cm inside the separatrix, representative of diverted plasma configurations. In the case of limited plasmas, the sharp increases of g_X would be centered on the last closed flux surface radius, which will not significantly change the results shown here, assuming that the frozen SOL can be locally relaxed. Here we ignore, on purpose, any effect of the magnetic shear induced stress in the core region, so as to focus on the edge where the poloidal symmetry breaking is strong. The electrostatic flow equilibrium is computed for favorable and unfavorable configurations, using Eqs.5 & 6 for the stress. The main difference appears near the position of the step of the function

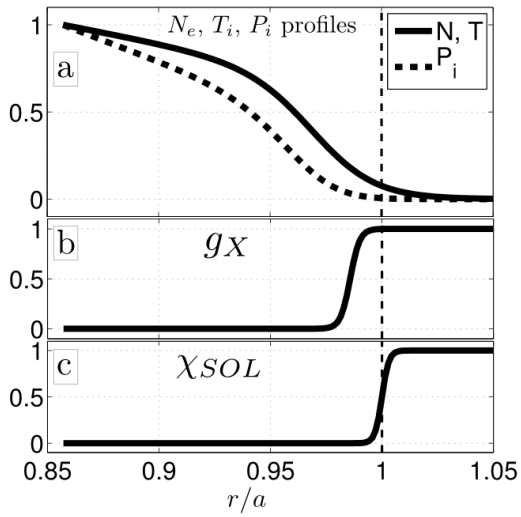

Figure 4. Frozen profiles. **a**: Density, temperature and pressure profiles (normalized to the core value). **b** : profile of g_X (resistive X-point penetration) : the confined region is supposed resistive within 1cm inside the LCFS. **c** : profile of SOL forcing function

g_X, i.e at the transition between minimal $\Pi_{\hat{s}}$ stress in the core and maximal $\Pi_{\hat{s}}$ stress at the edge boundary. The results are summarized in figure 5. Two extremal envelope shapes have been considered, a Gaussian of half width $\Delta\theta = 50^o$ and a flute mode. If the envelope width drops to zero, $\Pi_{\hat{s}}$ and $\Pi_{V_E'}$ should vanish and the radial electric field in both configurations should converge toward the same equilibrium profile obtained without the shear induced stress. The departure from this profile should be maximum for flute-modes.

Approaching the core, the Reynolds force tends to zeros and we effectively recover the previous relation $V_E = -V_i^*$. Toward the separatrix, we observe a progressive separation in the profiles. In the favorable (unfavorable) configuration, the Reynolds force acts as a positive (negative) source of perpendicular torque one centimeter inside the LCFS (see also figure 6), near the position where the X-point resistivity changes. The Reynolds force peak is dominated by the magnetic shear residual stress. Note also on figure 6 that the Reybolds force reverses sign closer to the LCFS.

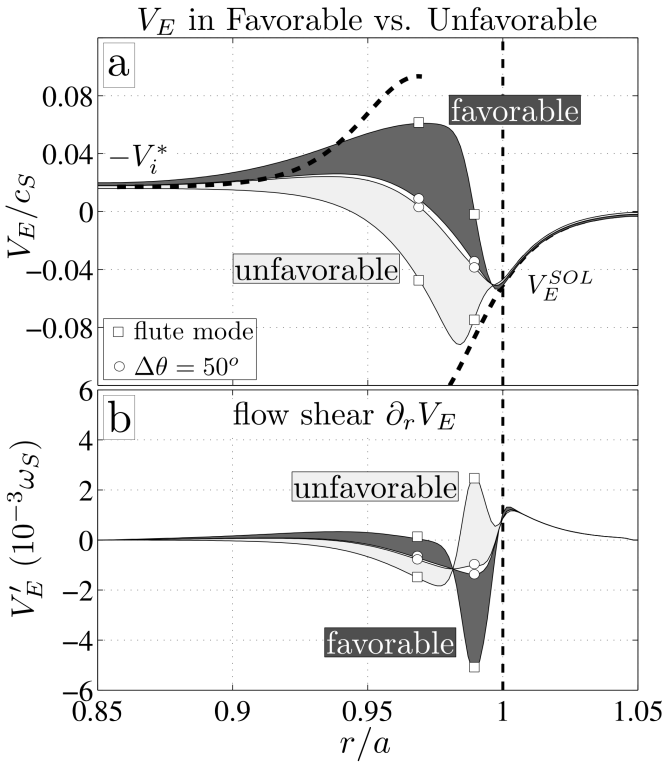

Figure 5. a: radial profile of electrostatic velocity for unfavorable (light gray) and favorable (dark gray) configurations. The core diamagnetic velocity and SOL electrostatic velocity are shown in dashed lines (boundary conditions). The extremal profiles (squares) correspond to flute modes and the interior profiles (circles) correspond to a Gaussian envelope $\Delta\theta = 50^o$. **b** Associated electric shear. Again the flute mode gives the exterior contour lines and the thin Gaussian the interior lines.

This tends to accentuate the $E \times B$ shear that would exist without turbulence. If the geometry is reversed, the magnetic shear induced Reynolds force also reverses and the contribution to the $E \times B$ shear now competes with the natural profile. The favorable configuration profile exhibits a shear strength about two times larger than the unfavorable shear at the same position. Its strength is about $|V_E'|\tau_c/\hat{s} \leq 0.2$, which is consistent with the weak shear assumption followed from the beginning. The difference between unfavorable and favorable electric velocity profiles is

in good agreement with experimental results obtained in the Tokamak Tore Supra [14].

In that experiment, a circular, ohmically heated plasma is limited either below or above the outboard midplane ($\theta_X = \pm 40^o$), by a set of discrete limiters that can be considered to be almost uniform toroidally. These limiter configurations are geometrically equivalent to favorable and unfavorable configurations for diverted plasmas. The electric field profile is estimated at the edge by Doppler back-scattering [39]. In the far SOL, the electric field does not depend on the limiter configuration, and is directed outward. Approaching the core, it recovers the neo-classical direction, i.e directed inward. In the vicinity of the last closed flux surface, a significant difference appears between the two limited configurations. When the limiter position is changed from below (favorable with respect to the magnetic field direction) to above the midplane (unfavorable), the transversal velocity amplitude measured across the last closed flux surface drops by a few percent of the ion sound speed, with a profile modification similar to the change predicted by the model (figure 5). The pressure profile does not change significantly with the limiter configuration, neither do any macroscopic quantities except the volume integral of the parallel flows in the SOL. The magnetic shear induced Reynolds stress is a potentially good candidate to explain the change of electric shear strength observed in this experiment. The sign of the source of transversal rotation in the vicinity of the separatrix, has pictured by the model, is also in agreement with what is required to explain the differences observed by beam emission spectroscopy in L-mode plasmas performed in DIII-D [13].

One important output of this model is not only that it can produce a weaker edge electrostatic shear in unfavorable than in favorable L-mode plasma configurations, but that the effect is due

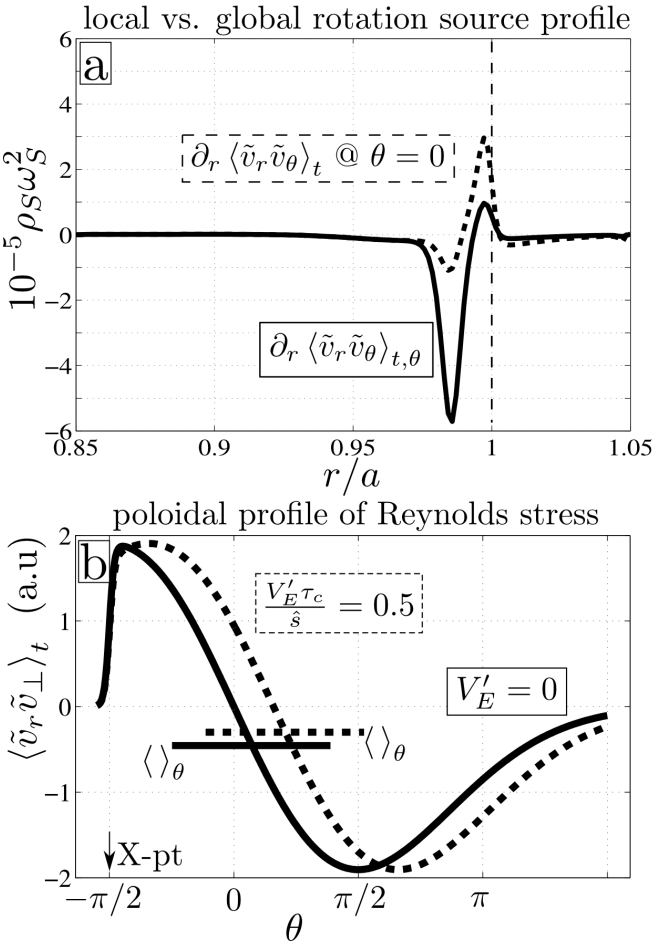

Figure 6. **a**: Radial derivative of the Reynolds stress across the profile for a favorable configuration with a ballooning envelope of half width $\Delta\theta = 90^o$, averaged over the flux surface (full curve) or taken locally at the outboard midplane (dashed line). **b** : Reynolds stress variation on a flux surface where the resistive X-point effect acts, for a zeros (full curve) or a positive (dashed curve) local electric shear. The amplitudes of the poloidal average of the stress are also shown.

to a Reynold stress that is not poloidally symmetric, as shown on figure 6. As a consequence, a measurement of the electric stress $\langle \tilde{v}_r \tilde{v}_\theta \rangle_t$ performed at one single poloidal location on a flux surface can not completely determine the flux surface averaged value. This important property is illustrated in figure 6**a**, where the radial derivative of the Reynolds stress taken at the outboard midplane is compared to its average over the flux surface. Although the position of maximum

source for the sheared flow are similar *in that particular example*, the local measurement is 3 times lower in amplitude than the flux surface averaged value. More generally, the local Reynolds stress amplitude is not related to its poloidal average, as shown on figure 6**b** where are shown two poloidal distributions of the Reynolds stress at two different electric shear values. Estimating the real momentum source on a flux surface therefore requires to reconstruct the poloidal dependence of the Reynolds stress via measurements at different poloidal positions. Here we point out that the poloidal variation shown on figure 6**b** is model dependent and only reflects a potential trend that could be inferred from experiments. The real shape of the flux surfaces will imply an additional asymmetry of the ballooning envelope and so for the Reynolds stress. But in any cases, it is pointed out here that the Reynolds stress can effectively vary by several units and reverses sign along a flux surface.

Before concluding on this study, we also report on the direct application of this model to the calculation of a residual stress for the toroidal rotation.

5. Discussion on the source of toroidal flow at the edge

In this section, we are concerned with intrinsic toroidal rotation and the effects of the shear induced stress on toroidal flows. Thus, we require the contribution of the perpendicular stress $\langle \tilde{v}_r \tilde{v}_\perp \rangle$ to the toroidal Reynolds stress $\langle \tilde{v}_r \tilde{v}_\phi \rangle$. This is determined by a simple toroidal projection:

$$\langle \tilde{v}_r \tilde{v}_\phi \rangle = -\frac{B_\theta}{B} \langle \tilde{v}_r \tilde{v}_\perp \rangle$$

Observe this is equivalent to writing the $\langle J_r \rangle \langle B_\theta \rangle / c$ force which acts on the toroidal direction, since $\langle J_r \rangle \equiv -\partial_r \langle \tilde{v}_r \tilde{v}_\theta \rangle$ [1]. Of course, the total toroidal Reynolds stress includes several other

contributions, i.e.

$$\langle \tilde{v}_r \tilde{v}_\phi \rangle = \frac{B_T}{B} \langle \tilde{v}_r \tilde{v}_{||} \rangle - \frac{B_\theta}{B} \left(\langle \tilde{v}_r \tilde{v}_\perp \rangle|_{\hat{s}} + \langle \tilde{v}_r \tilde{v}_\perp \rangle|_{V_E'} + ... \right)$$

In particular, the parallel Reynolds stress includes the effect of SOL flow induced radial penetration of parallel flow in the confined plasma, as suggested by LaBombard [18]. This inward transport could be affected by parallel shear flow instability of the SOL flow, resulting in inward diffusive transport. These SOL induced flows will have large toroidal component, since $B_T \gg B_\theta$, and so will potentially drive a toroidal flow shear layer. Another contribution to $\langle \tilde{v}_r \tilde{v}_{||} \rangle$ is due to $\langle V_E \rangle'$ symmetry breaking, leading to $\langle k_\theta k_{||} \rangle \neq 0$ and a finite residual $\langle \tilde{v}_r \tilde{v}_{||} \rangle \neq 0$ [40], which is now well known to drive intrinsic rotation. Last but not least, it is reminded that the shear induced stress studied here as a result of a poloidal symmetry breaking can find some analogies with the radial/parallel stress described in [24], although the mechanism is completely different. The amplitude of a residual term C_Φ entering the flux of parallel rotation is estimated in the form $\Gamma_\Phi = \chi_\Phi^{eff} u' + C_\Phi$. The dimensionless differential rotation is defined as $u' = R^2 \partial_r \Omega_\Phi / c_S$ with R the plasma major radius and Ω_Φ the toroidal angular velocity. It is also mentioned that the toroidal momentum viscosity is approximately equal to the ion diffusivity, so that within their normalization $\chi_\Phi^{eff} \approx c_S^2 \frac{\rho_S}{R} \frac{\rho_S}{L_T}$ [37], where L_T is the temperature gradient length. The amplitude of the residual term is comparable to the viscous term $C_\Phi / \chi_\Phi^{eff} \approx 1$. On the other hand, the toroidal projection of the transversal shear induced stress presented in our paper is on the order of $C_\Phi^\perp = \alpha \frac{B_\theta}{B_T} \langle \tilde{v}_r^2(0) \rangle_t$ with α of order unity. Applying the same comparison as in [24] gives :

$$C_\Phi^\perp / \chi_\Phi^{eff} \approx \frac{B_\theta}{B_T} \frac{L_T}{R} \left(\frac{R}{\rho_S} \right)^2 \frac{\langle \tilde{v}_r^2(0) \rangle_t}{c_S^2}$$

For normal plasma conditions used here and in their paper: $\frac{B_\theta}{B_T} \approx 0.1$, $\frac{L_T}{R} \approx 0.1$, $\frac{\langle \tilde{v}_r^2(0) \rangle_t}{c_S^2} \approx 10^{-4}$ (coherent with the temperature gradient scale length from Mattor scalings [37]) and $\frac{R}{\rho_s} \approx 10^3$, we estimate that our flux of toroidal momentum also scales like $C_\Phi^\perp / \chi_\Phi^{eff} \approx 1$. Note that both effects are not identical and therefore accumulate. Thus the toroidal projection of the shear induced Reynolds stress also appears as a potentially significant contribution for the intrinsic toroidal rotation:

$$\Pi_\phi = -\frac{B_\theta}{B_T} \left[\Pi_{\hat{s}} + \Pi_{V_E'} \right]$$

In the following we focus only on the effects of the toroidal projection of perpendicular stresses. Referring to the work of Diamond *et al.* on the intrinsic toroidal rotation in a tokamak [41], this stresses enter the momentum balance via the relation:

$$\partial_t \langle V_\phi \rangle = +\chi_\phi \partial_r^2 \langle V_\phi \rangle - \partial_r \Pi_\phi$$

where we omitted a pinch term. In steady state, momentum conservation implies that the flux of toroidal momentum at the boundary of the confinement region is zero, which fixes the gradient of toroidal velocity to balance the residual stress, i.e.

$$\partial_r \langle V_\phi \rangle|_{r=a} = - \left. \frac{B_\theta}{B_T} \frac{\Pi_{\hat{s}} + \Pi_{V_E'}}{\chi_\phi} \right|_{r=a}$$

In favorable configurations with I_P co-aligned with B_T, the shear residual stress is, in the weak shear regime, negative. This will force the toroidal velocity gradient is to be positive at the boundary of the confined region, in the order of $\partial_r \langle V_\phi \rangle|_{r=a} \approx$km.s^{-1}.cm^{-1}. This is observed in Tore Supra experiments [14] and also in DIII-D for L-mode ohmically heated plasmas [42]. That said, changing to unfavorable configuration would reverse the sign of the stress and so of the velocity gradient, suggesting that the toroidal rotation in the bulk plasma should be higher in

unfavorable than favorable geometries, *if the velocity at the boundary in not significantly changed.* However, experiments show that the core toroidal rotation is more counter current in unfavorable than favorable geometries [43], which points toward additional residual stress mechanisms at least in the core region. One possibility is discussed in [44]. In particular, the core turbulence generates a local intrinsic torque ($-\partial_r \langle \tilde{v}_r \tilde{v}_\phi \rangle$), the sign of which is determined by profile structure and mode propagation direction. Changes in core rotation direction in L-mode are associated with changes in density, current and confinement scaling [45]. Thus, the *net* rotation profile is set by a confluence of many factors, including edge layer and SOL torques, core residual stress, etc. A global momentum transport study is required to resolve this question.

6. summary

At the edge of an L-mode tokamak plasma where ballooning structures are likely to dominate the transport, the time averaged Reynolds stress $\langle \tilde{v}_r \tilde{v}_\perp \rangle_t$ includes a residual component, not proportional to the mean flow nor its gradient. One part of this stress is the consequence of spatial tilting of ballooning modes excited at the outboard midplane $\langle \tilde{v}_r \tilde{v}_\perp \rangle_t = \langle \tilde{v}_r^2 \rangle_t [V_E' \tau_c - \hat{s}\theta]$. The tilt due to the electric shear refers to a negative viscosity term. The tilt due to the magnetic shear $\hat{s}$, or $\hat{s}$-residual stress, is locally proportional to the poloidal position where it is considered, and thus exhibits an anti-symmetric pattern with respect to the midplane. A ballooning envelope with an up-down asymmetry will induce a net asymmetry in the poloidal distribution of the momentum flux, creating a non-vanishing flux surface averaged stress. Due to the presence of parallel boundary conditions in the SOL, and because of the exponentially enhanced cross field decorrelation rate in the vicinity of an X-point, an asymmetry of the ballooning envelope develops

at the very edge. It applies both to toroidally symmetric limited plasma and X-point plasma configurations. Besides, the non-linear dependence of this $\hat{s}$-residual stress on the local flow shear is investigated via the impact of the flow shear on the ballooning envelope. A model is proposed for the Gaussian ballooning envelope poloidally shifted by the flow shear at the peaking position $\theta_0 = V'_E \tau_c / \hat{s}$. The flux surface averaged residual stress is found to be of the order of the square of the electrostatic radial velocity fluctuations $\langle \tilde{v}_r^2 \rangle_{t,\theta}$, and its sign also reverses when the magnetic geometry is changed from favorable ($B \times \nabla B$ toward the X-point) to unfavorable ($B \times \nabla B$ away from the X-point) geometry, i.e. $\Pi_{\hat{s}}^{USN}(V'_E) = -\Pi_{\hat{s}}^{LSN}(-V'_E)$. It's absolute amplitude should also decrease with the plasma triangularity. Its impact on the L-mode edge velocity shear is illustrated through a simplified model of perpendicular momentum conservation at the plasma edge, including SOL boundary conditions. The flow shear in the vicinity of the separatrix is two times lower in amplitude for unfavorable than for favorable configuration, in qualitative agreement with experimental results. The reason is a favorable or unfavorable competition between equilibrium $E \times B$ shear and turbulent driven shear. The Reynolds force is strongly non uniform poloidally, and can not be directly inferred from a single point measurement.

This shear induced stress for perpendicular rotation also determines a residual stress for toroidal rotation in the vicinity of the last closed flux surface. It potentially adds to and may compete with other source mechanisms, like SOL flows penetration, ion orbit losses and other symmetry breaking based residual fluxes of parallel momentum.

Validation of this model requires measurements of the Reynolds stress away form the outboard midplane as done in [28], in order to determine the magnetic shear tilting. Further developments

of the model require a more accurate description of the ballooning envelope in a real plasma geometry, including plasma shaping and the envelope response to a sheared flow. This can only be quantified precisely by 3D calculations about the plasma region surrounding the separatrix, as initiated in [46]. In fact, an extended version of this model should address the issue of defining an optimal plasma shape maximizing the $\hat{s}$-residual stress, accentuating the L-mode flow shear and thus lowering the L to H-mode transition power threshold. This is already addressed from the point of view of penetration of SOL flows into the core [18], but a more complete story should include other potential mechanisms sensitive to flux surface topology. Finally, to address L-H transition physics, this model must include both zonal and mean (diamagnetic) shear effects and shearing feedback on fluctuation intensity.

7. acknowledgement

This work was supported by the United States D.O.E. and the W.C.I Program of the republic of Korea. The authors are grateful to the participants of Festival de théorie 2011, organized by the C.E.A of France, for many valuable discussions. We especially thank Özgur Gürcan and Pascale Hennequin for enlightening discussions.

[1] P. H. Diamond and Y.-B. Kim. *Physics of Fluids B: Plasma Physics*, 3(7):1626–1633, 1991.

[2] F Wagner. *Plasma Physics and Controlled Fusion*, 49(12B):B1, 2007.

[3] Eun-jin Kim and P. H. Diamond. *Phys. Rev. Lett.*, 91:075001, 2003.

[4] P H Diamond, S-I Itoh, K Itoh, and T S Hahm. *Plasma Physics and Controlled Fusion*, 47(5):R35, 2005.

[5] K. H. Burrell. *Physics of Plasmas*, 4(5):1499–1518, 1997.

[6] T. Estrada, E. Ascasbar, T. Happel, C. Hidalgo, E. Blanco, R. Jimnez-Gmez, M. Liniers, D. Lpez-Bruna, F.L. Tabars, and D. Tafalla. *Contributions to Plasma Physics*, 50(6-7):501–506, 2010.

[7] S. J. Zweben, R. J. Maqueda, R. Hager, K. Hallatschek, S. M. Kaye, T. Munsat, F. M. Poli, A. L. Roquemore, Y. Sechrest, and D. P. Stotler. *Physics of Plasmas*, 17(10):102502, 2010.

[8] G. D. Conway, C. Angioni, F. Ryter, P. Sauter, and J. Vicente. *Phys. Rev. Lett.*, 106:065001, 2011.

[9] K. Kamiya, K. Ida, Y. Sakamoto, G. Matsunaga, A. Kojima, H. Urano, N. Oyama, Y. Koide, and Y. Kamada. *Phys. Rev. Lett.*, 105:045004, 2010.

[10] Eun-jin Kim and P. H. Diamond. *Phys. Rev. Lett.*, 90:185006, 2003.

[11] G.R. McKee, P. Gohil, D.J. Schlossberg, J.A. Boedo, K.H. Burrell, J.S. deGrassie, R.J. Groebner, R.A. Moyer, C.C. Petty, T.L. Rhodes, L. Schmitz, M.W. Shafer, W.M. Solomon, M. Umansky, G. Wang, A.E. White, and X. Xu. *Nuclear Fusion*, 49(11):115016, 2009.

[12] J.A. Snipes, R.S. Granetz, M. Greenwald, O.J.W.F. Kardaun, A. Kus, F. Ryter, U. Stroth, J. Kollermeyer, S.J. Fielding, M. Valovic, J.C. DeBoo, T.N. Carlstrom, D.P. Schissel, K. Thomsen, D.J. Campbell, J.P. Christiansen, J.G. Cordey, E. Righi, Y. Miura, N. Suzuki, M. Mori, T. Matsuda, H. Tamai, T. Fukuda, Y. Kamada, T. Matsuda, M. Sato, T. Takizuka, K. Tsuchiya, and S.M. Kaye. *Nuclear Fusion*, 36(9):1217, 1996.

[13] T N Carlstrom, R J Groebner, C Fenzi, G R McKee, R A Moyer, and T L Rhodes. *Plasma Physics and Controlled Fusion*, 44(5A):A333, 2002.

[14] P. Hennequin, L. Vermare, N. Fedorczak, J. Bernardo, Ö.D. Gürcan, E. Trier, N. Stuyck, C. Fenzi, J. Gunn, P. Monier-Garbet, C. Bourdelle, P. Ghendrih, and X. Garbet. *European Physical Society*, P1.1040, 2010.

[15] R. Raman, J-W. Ahn, and J.P. Allain. *Nuclear Fusion*, 51(9):094011, 2011.

[16] T. E. Stringer. *Phys. Rev. Lett.*, 22:770–774, 1969.

[17] A. B. Hassam, Jr. T. M. Antonsen, J. F. Drake, P. N. Guzdar, C. S. Liu, D. R. McCarthy, and F. L. Waelbroeck. *Physics of Fluids B: Plasma Physics*, 5(7):2519–2524, 1993.

[18] B. LaBombard, J.E. Rice, A.E. Hubbard, J.W. Hughes, M. Greenwald, J. Irby, Y. Lin, B. Lipschultz, E.S. Marmar, C.S. Pitcher, N. Smick, S.M. Wolfe, S.J. Wukitch, and the Alcator Group. *Nuclear Fusion*,

44(10):1047, 2004.

[19] J.P. Gunn, C. Boucher, M. Dionne, I. uran, V. Fuchs, T. Loarer, I. Nanobashvili, R. Pnek, J.-Y. Pascal, F. Saint-Laurent, J. Stckel, T. Van Rompuy, R. Zagrski, J. Admek, J. Bucalossi, R. Dejarnac, P. Devynck, P. Hertout, M. Hron, G. Lebrun, P. Moreau, F. Rimini, A. Sarkissian, and G. Van Oost. *Journal of Nuclear Materials*, 363365(0):484 – 490, 2007.

[20] N. Fedorczak, J. P. Gunn, J.-Y. Pascal, Ph. Ghendrih, Y. Marandet, and P. Monier-Garbet. *Physics of Plasmas*, 19(7):072313, 2012.

[21] N. Fedorczak, J.P. Gunn, Ph. Ghendrih, G. Ciraolo, H. Bufferand, L. Isoardi, P. Tamain, and P. Monier-Garbet. *Journal of Nuclear Materials*, 415(1, Supplement):S467 – S470, 2011.

[22] G. Birkenmeier, M. Ramisch, P. Manz, B. Nold, and U. Stroth. *Phys. Rev. Lett.*, 107:025001, 2011.

[23] G R Tynan, J Liberati, P Pribyl, R J Taylor, and B Wells. *Plasma Physics and Controlled Fusion*, 38(8):1301, 1996.

[24] Y. Camenen, A. G. Peeters, C. Angioni, F. J. Casson, W. A. Hornsby, A. P. Snodin, and D. Strintzi. *Phys. Rev. Lett.*, 102:125001, 2009.

[25] Y. Sarazin and Ph. Ghendrih. *Physics of Plasmas*, 5(12):4214–4228, 1998.

[26] P. Beyer, S. Benkadda, X. Garbet, and P. H. Diamond. *Phys. Rev. Lett.*, 85:4892–4895, 2000.

[27] J.L. Terry, S.J. Zweben, M.V. Umansky, I. Cziegler, O. Grulke, B. LaBombard, and D.P. Stotler. *Journal of Nuclear Materials*, 390391(0):339 – 342, 2009.

[28] N. Fedorczak, J. P. Gunn, J.-Y. Pascal, Ph. Ghendrih, G. van Oost, P. Monier-Garbet, and G. R. Tynan. *Physics of Plasmas*, 19(7):072314, 2012.

[29] V S Mikhailenko, V V Mikhailenko, and K N Stepanov. *Plasma Physics and Controlled Fusion*, 52(5):055007, 2010.

[30] A. Loarte and P.J. Harbour. *Nuclear Fusion*, 32(4):681, 1992.

[31] J. R. Myra, D. A. D'Ippolito, X. Q. Xu, and R. H. Cohen. *Physics of Plasmas*, 7(6):2290–2293, 2000.

[32] F.L Waelbroeck and L Chen. *Phys. Fluids B*, 3, 1991.

[33] Y. Camenen, Y. Idomura, S. Jolliet, and A.G. Peeters. *Nuclear Fusion*, 51(7):073039, 2011.

[34] Y. Camenen, A. G. Peeters, C. Angioni, F. J. Casson, W. A. Hornsby, A. P. Snodin, and D. Strintzi. *Physics of Plasmas*, 16(6):062501, 2009.

[35] E. Trier, L.-G. Eriksson, P. Hennequin, C. Fenzi, C. Bourdelle, G. Falchetto, X. Garbet, T. Aniel, F. Clairet, and R. Sabot. *Nucl. Fusion*, 48(9):092001, 2008.

[36] A.V. Chankin, D.P. Coster, N. Asakura, X. Bonnin, G.D. Conway, G. Corrigan, S.K. Erents, W. Fundamenski, J. Horacek, A. Kallenbach, M. Kaufmann, C. Konz, K. Lackner, H.W. Mller, J. Neuhauser, R.A. Pitts, and M. Wischmeier. *Nuclear Fusion*, 47(5):479, 2007.

[37] N. Mattor and P. H. Diamond. *Physics of Fluids B: Plasma Physics*, 1(10):1993–1997, 1989.

[38] H. Biglari, P.H. Diamond, and P.W. Terry. *Phys. Fluids B*, 2, 1990.

[39] P. Hennequin, C. Honor, A. Truc, A. Qumneur, C. Fenzi-Bonizec, C. Bourdelle, X. Garbet, G.T. Hoang, and the Tore Supra team. *Nuclear Fusion*, 46(9):S771, 2006.

[40] Ö. D. Gürcan, P. H. Diamond, T. S. Hahm, and R. Singh. *Physics of Plasmas*, 14(4):042306, 2007.

[41] P.H. Diamond, C.J. McDevitt, .D. Grcan, T.S. Hahm, W.X. Wang, E.S. Yoon, I. Holod, Z. Lin, V. Naulin, and R. Singh. *Nuclear Fusion*, 49(4):045002, 2009.

[42] S. H. Müller, J. A. Boedo, K. H. Burrell, J. S. deGrassie, R. A. Moyer, D. L. Rudakov, and W. M. Solomon. *Phys. Rev. Lett.*, 106:115001, 2011.

[43] J.E. Rice, A.C. Ince-Cushman, M.L. Reinke, Y. Podpaly, M.J. Greenwald, B. LaBombard, and E.S. Marmar. *Plasma Phys. Control. Fusion*, 50(12):124042, 2008.

[44] J. E. Rice, J. W. Hughes, P. H. Diamond, Y. Kosuga, Y. A. Podpaly, M. L. Reinke, M. J. Greenwald, Ö. D. Gürcan, T. S. Hahm, A. E. Hubbard, E. S. Marmar, C. J. McDevitt, and D. G. Whyte. *Phys. Rev. Lett.*, 106:215001, 2011.

[45] J.E. Rice, B.P. Duval, M.L. Reinke, Y.A. Podpaly, A. Bortolon, R.M. Churchill, I. Cziegler, P.H. Diamond, A. Dominguez, P.C. Ennever, C.L. Fiore, R.S. Granetz, M.J. Greenwald, A.E. Hubbard, J.W. Hughes, J.H. Irby, Y. Ma, E.S. Marmar, R.M. McDermott, M. Porkolab, N. Tsujii, and S.M. Wolfe. *Nuclear Fusion*, 51(8):083005, 2011.

[46] D.A. Baver, J.R. Myra, and M.V. Umansky. *Computer Physics Communications*, 182(8):1610 – 1620, 2011.